Int. J. Solids Structures Vol. 14, pp. 739–753
© Pergamon Press Ltd., 1978. Printed in Great Britain

0020–7683/78/0901–0739/$02.00/0

MEASUREMENT OF DYNAMIC MATERIAL BEHAVIOR UNDER NEARLY UNIAXIAL STRAIN CONDITIONS†

BHARAT BHUSHAN‡§ and W. E. JAHSMAN¶
Department of Mechanical Engineering, University of Colorado, Boulder, CO 80309, U.S.A.

(*Received* 3 *January* 1978; *received for publication* 13 *March* 1978)

Abstract—The conventional Kolsky apparatus (split Hopkinson pressure bar), normally used to obtain dynamic material behavior in uniaxial stress, has been modified to provide conditions approaching uniaxial strain. The modification consists of a massive steel collar which surrounds the disk-shaped specimen and suppresses its radial motion. The collar is composed of two concentric steel cylinders, each 160 mm long; an outer thick-walled jacket of low-carbon steel with an OD of 200 mm and a wall thickness of 75 mm; and an inner liner of AT-300 maraging steel which is press-fitted into the jacket. The ID of the liner is nominally 38 mm, and is slightly flared to allow easy insertion of the specimen. Very close tolerances are maintained between the liner minimum diameter and the specimen diameter; differences in liner and specimen diameters normally do not exceed 2.5 μm. For testing purposes, the specimen is first inserted in the collar and then the specimen/collar assembly is placed between the input and output bars of the Kolsky apparatus. A bell-shaped stress pulse of approximately 40 μs duration and 1.28 GPa amplitude is propagated along the input bar, and a portion of this pulse is transmitted through the specimen into the output bar. Records of strain histories are taken on the input and output bars as well as on the outside of the collar. Data reduction utilizes the conventional Kolsky formulas for the determination of axial stress and strain histories in the specimen, and a supplementary equation has been developed to calculate the radial stress history for ductile metallic specimens.

Tests were conducted on both metallic and nonmetallic materials. In the former category, three different aluminum alloys—3003 (as machined or annealed), 2024-T351 and 6061-T651 and oxygen-free copper were tested. Comparisons were made with static test results for these same materials. It was found that the collar provides considerable restraint against radial motion, with an effective modulus of approximately 280 GPa. Significant differences were found between the static and dynamic curves in spite of the fact that loading configurations were identical for both sets of tests. The differences are attributed to strain rate effects, low-temperature creep and differences in the dynamic and static stress histories. Similar trends were observed for dynamic and static measurements made with the collar removed (nearly uniaxial stress condition). In the non-metallic material category, Scotchply, syntactic foam and polypropylene panels were tested. In each case, dramatic differences between static and dynamic behavior of the unconstrained specimens were observed, while the constrained specimens exhibited little or even apparent reverse strain-rate effects.

1. INTRODUCTION

Over the past 25 years, the Kolsky apparatus[1] has become a standard device for the determination of dynamic compressive[2] and tensile[3] properties of a variety of materials at strain rates of 10^{+3} s^{-1}. With careful attention to the length-to-diameter ratio of the specimen[4], and with generous amounts of lubricant on the specimen faces, investigators have been able to achieve a state of nearly uniaxial stress in the specimen. More recently, a pure shear stress state has been approached in tubular specimens[5,6] through the development of a torsional counterpart to the original Kolsky apparatus. A lucid stress state is also achieved with the sophisticated and expensive "plate slap" devices which produce uniaxial strain conditions[7]. In these tests a plane shock wave is introduced into the specimen, and the strain rates are several orders of magnitude above those produced in the conventional Kolsky systems.

A review of the literature reveals that no attempt has been made to modify the Kolsky apparatus to achieve nearly uniaxial strain conditions. This omission is surprising in view of the simplicity of the modification, a massive collar to suppress radial motion in the disk-shaped specimen. Accordingly, a collar has been machined and installed in the Kolsky apparatus operated at the University of Colorado[8]. Dynamic tests have been conducted on a series of

†Presented at the 8*th U.S. Nat. Cong. Appl. Mech.*, University of California, Los Angeles, 26–30 June 1978.
‡Presently at: Mechanical Technology Incorporated 968 Albany-Shaker Road, Latham, NY 12110, U.S.A.
§Research Assistant and Instructor.
¶Professor and Chairman.

metallic and non-metallic materials, and comparisons have been made with previous tests on unconstrained specimens and with static data.

2. EXPERIMENTAL APPARATUS AND PROCEDURE

2.1 *Modified Kolsky apparatus*

The principal elements are illustrated schematically in Fig. 1 and a photograph of the complete setup is shown in Fig. 2. The apparatus consists of four main mechanical components: the driver, the input and output bars, the momentum trap, and the collar. The driver features an air gun which is designed to operate at pressures up to 14 MPa to accelerate a steel impactor. The impactor is a short cylindrical bar of maraging steel, 38 mm in diameter and 50 mm in length.

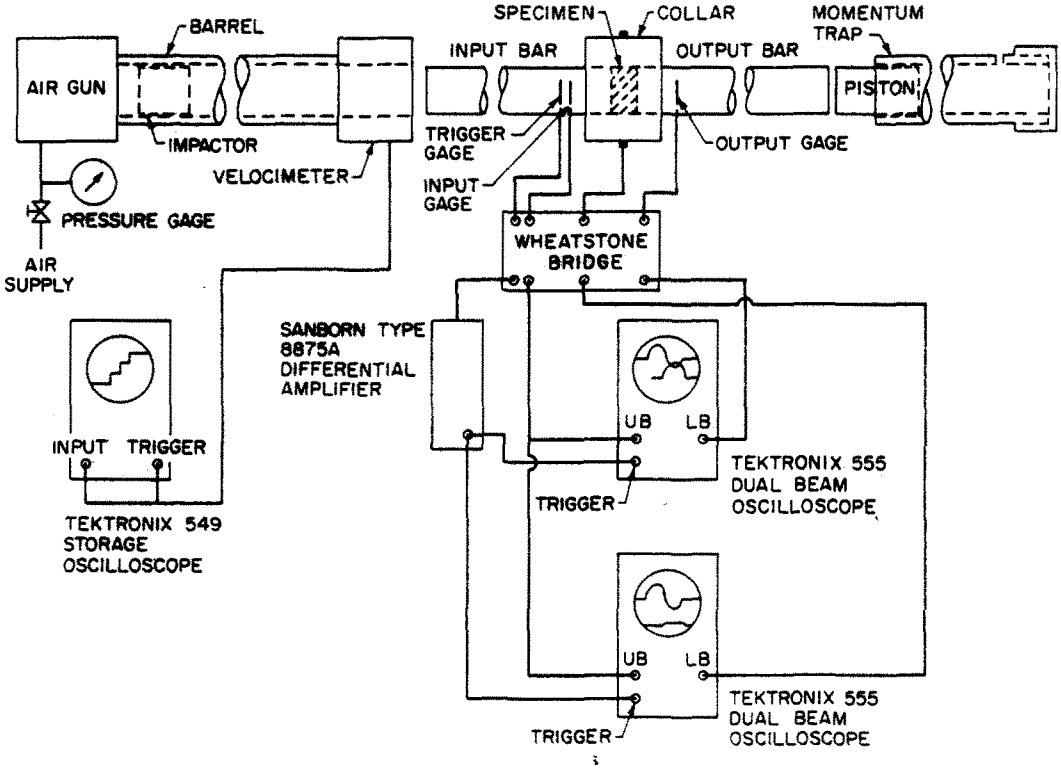

Fig. 1. Schematic arrangement of the collar-modified Kolsky apparatus.

Speed of the impactor just prior to striking the input bar is measured by means of a velocimeter. The input and output bars were cut from AT-300 maraging steel stock with a guaranteed minimum yield strength of 1.9 GPa. The bars are 0.91 m long and 38 mm in diameter and are supported in low acoustic impedance nylon bushings. Faces of the bars were carefully machined and ground to assure parallel contact with the impactor and momentum trap piston at the outer ends and with the specimen in between.

Records of circumferential strain histories were obtained by means of pairs of diametrically opposed semiconductor gages mounted at distances of 100 mm from the ends of the bars in contact with the specimen. Orientation of the gages—with the narrow dimension (2.3 mm) in the direction of wave propagation—assures minimum integration of the signal over the gage length. The gages were connected through separate Wheatstone bridges to the vertical inputs of the two beams of a Tektronix 555 oscilloscope. Triggering for both beams was provided by a separate set of diametrically opposed semiconductor gages mounted 25 mm ahead of the input gages. All semiconductor gages are Kulite type DLP-120-500 with a nominal gage factor of 55.

A substantial portion of the energy in the pulse transmitted into the output bar was captured in the momentum trap located at the far end of the output bar. The pneumatic shock absorber principle is used in the momentum trap, with air escaping through an orfice.

The collar consists of two concentric cylinders, each 160 mm long. The outer jacket was

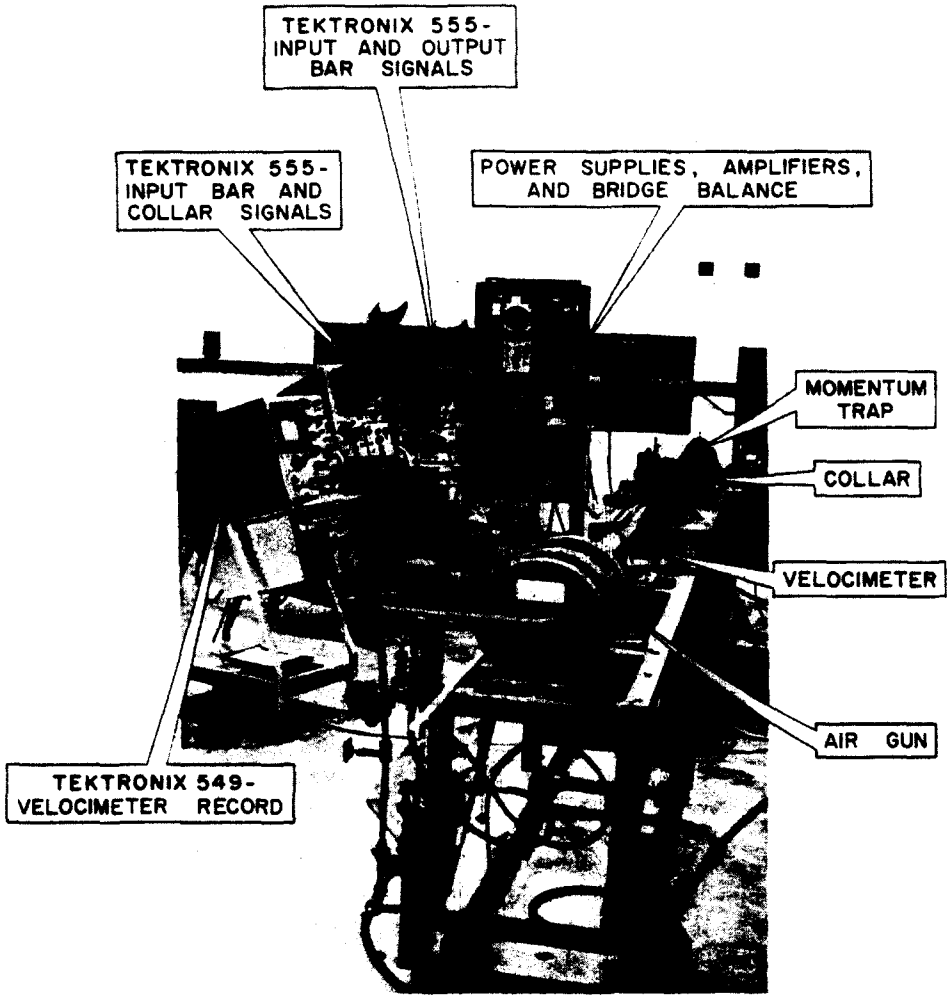

Fig. 2. Photograph of the collar-modified Kolsky apparatus.

machined from low-carbon steel stock. Press-fitted into this jacket is a maraging steel liner. Although a substantial portion of the inner diameter of the liner was carefully machined to 38.2981 ± 0.0010 mm, a slight flare was introduced over the outer 25 mm of length at each end of the liner to facilitate insertion and removal of the test specimen.

As seen in Fig. 2, the collar rests on a dolly which rides on tracks. The tracks are mounted rigidly to the test bed which holds the input and output bars. Nominal care was exercised in orienting the tracks perpendicular to the bars. Final adjustment was made through alignment of the input and output bar supports.

Collar instrumentation consists of diametrically opposed semiconductor strain gages mounted at the midlength of the outer circumference of the collar (Fig. 2). Geometric attenuation between the specimen/liner interface and the outside of the jacket is substantial (on the order of 58 under static conditions, see Ref. [9]), and high amplification was required to detect the signal. Considerable noise, unobservable at normal amplification levels, was picked up and thus reduced the accuracy of the reading. Additional development is required before reliable, accurate readings will be available.

2.2 *Test procedure and data reduction*

Three major steps were required to obtain the experimental data. The first step involved the careful insertion of the specimen into the collar followed by the mounting of the collar/specimen assembly between the input and output bars. The circumferential and end surfaces of the specimen and the inner diameter of collar were lubricated with molybdenum dilufide in order to minimize the interfacial friction between the bars and the specimen and the specimen

and the collar. Because of the snug fit between specimen and collar, metallic specimens were cooled in a deep freeze before insertion. Temperatures were allowed to equalize before tests were initiated. For the syntactic foam specimens, shims were used to achieve the required fit. The amount of specimen prestress due to the interference fit was judged to be negligible since a force of on the order of 10 N was sufficient to dislodge the specimen. By contrast, forces three orders of magnitude greater than this were needed to remove metallic specimens following the test. A special tool was used to assure that the specimen was centered in the collar and parallel with the collar and faces.

After the collar/specimen assembly was properly mounted on the test bed, the impactor was loaded into the breech of the air gun and the lengthly process of alignment was carried out. In the third step, the air chamber in the air gun was pressurized. A pressure range of 200–700 kPa was found to be adequate for impactor velocities of interest. The momentum trap was placed firmly in contact with the far end of the output bar, and the velocimeter circuit and the oscilloscope trigger circuits were activated. The gun was then fired.

As mentioned previously, noise caused a serious problem because of the high gain needed with the collar gages. Hence, most signals were not suitable for permanent photographic records. A representative trace is shown in Fig. 3 for oxygen-free copper. For comparison, input and output gage signals are also presented. Note that the amplification for the collar gages is 20 times that needed for the bar gages.

The average axial stress and strain histories in the specimen [$\bar{\sigma}_z(t)$ and $\bar{\epsilon}_z(t)$] are obtained from the Kolsky formulas

$$\bar{\sigma}_z(t) = \frac{1}{2}[\sigma_i(t) + \sigma_{re}(t + t_d) + \sigma_0(t + t_d)] \tag{1}$$

$$\bar{\epsilon}_z(t) = \frac{2}{\rho_b c_b h}\int_0^t [\sigma_i(t') - \bar{\sigma}_z(t')]\,dt'. \tag{2}$$

The variables appearing in eqns (1) and (2) are σ_i, σ_{re} and σ_0, the axial stress histories obtained from the input and output bar strain gage records; ρ_b and c_b, the mass density and wave speed bars; h, the specimen thickness; and t_d, the travel time of the wave between input and output gages when the specimen is removed and the bars are placed in contact with one another. Repeated measurements show that the following values may be used with confidence for these parameters: $\rho_b = 8.14\,\text{kgl}^{-1}$, $c_b = 4.78\,\text{mm}\,\mu\text{s}^{-1}$, $h = 12.7\,\text{mm}$ and $t_d = 41.5\,\mu\text{s}$. For complete information on the (presumed) axisymmetric state of stress and strain, the radial stress and strain histories are needed. It was originally intended that the collar gages would provide this information; however, the poor accuracy of the signals has temporarily delayed that direct approach. As an alternative, an analysis was developed based on the radial dynamic impedance of the collar and the assumption that the specimen undergoes zero plastic volume change. Determination of the radial dynamic impedance was made from known static properties of the collar; the zero plastic volume change assumption limits the applicability of the analytical predictions to ductile metals at best. The result of this analysis, details of which are found in the Appendix, shows that the average radial stress history in the specimen [$\bar{\sigma}_r(t)$] and other parameters are given by

$$\bar{\sigma}_r(t) = \begin{cases} \left[\bar{\sigma}_r(t_1) + \frac{1}{2}\bar{\sigma}_z(t_1)\right] e^{-(t-t_1)/\tau_1} - \frac{1}{2}\bar{\sigma}_z(t) \\ + \frac{1}{\tau_1(1+\alpha)}\int_{t_1}^t \left[\chi\{\sigma_i(t') - \bar{\sigma}_z(t')\} + \frac{1}{2}\{E_c\bar{\epsilon}_z(t') + \sigma_0(t') + 2E_c\epsilon_1\}\right] e^{-(t-t')/\tau_1}\,dt', \\ \qquad t_1 < t < 2(b-a)/c_c \end{cases} \tag{3}$$

$$\bar{\sigma}_r(t_1) = \begin{cases} \chi\{\sigma_i(t_1) - \bar{\sigma}_z(t_1)\} - \tau_1(1+\alpha)\dot{\sigma}_z(t_1)/2, & \text{if} \\ \qquad\qquad \text{the specimen is rigid} \\ 0, \qquad\qquad \text{if the specimen is "soft"} \end{cases}$$

$$\sqrt{(J_2(t))} = \frac{1}{\sqrt{3}}(\bar{\sigma}_z(t) - \sigma_r(t)) \tag{4}$$

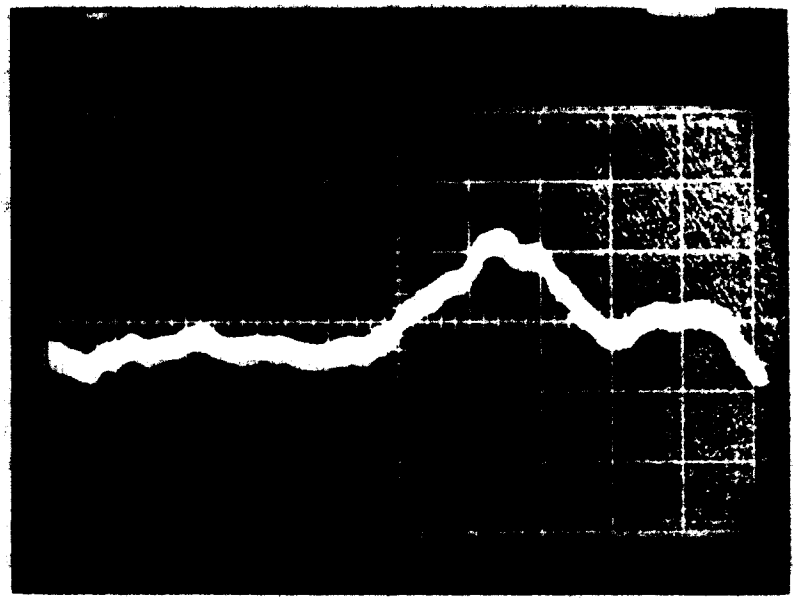

(a)

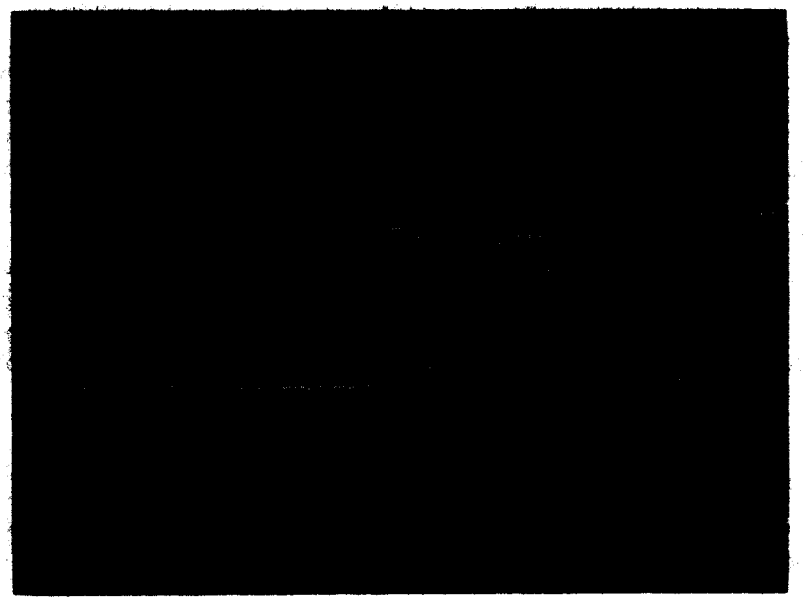

(b)

Fig. 3. Oscilloscope traces. (a) Collar gages (10 μs/10 mm sweep; 5 mV/10 mm deflection), (b) Input and output gages (10 μs/10 mm sweep; 0.1 V/10 mm deflection).

and

$$W^P(t) = \int_0^{\bar{\epsilon}_z^P(t)} \sqrt{(3J_2(t'))}\, \mathrm{d}\bar{\epsilon}_z(t')$$

$$\bar{\epsilon}_z^P(t) = \bar{\epsilon}_z(t) - \frac{1}{E_s}[\sigma_z(t) - 2\nu_s\bar{\sigma}_r(t)]. \tag{5}$$

The variables appearing in eqns (3)–(5) are ϵ_1, the ratio of the initial radial clearance between the specimen and collar to the specimen radius; t_1, the time required for the specimen to make contact with the collar; τ_1, a time parameter introduced for algebraic convenience and equal to $(a/c_c)\ \alpha/(1+\alpha)$; α, a collar to specimen stiffness ratio, $E_c(1-2\nu_s)/E_s$; c_c, effective wave speed in the collar, $\sqrt{(E_c/\rho_c)}$; E_c, effective collar modulus; and χ, the collar-to-bar impedance ratio, $(\rho c)_c\ a/(\rho c)_b h$. Equation (3) assumes that the collar impedance $(\rho c)_c$ remains constant throughout the propagation process. Reflections from the outer circumference of the collar will,

however, invalidate this assumption for times greater than $2(b-a)/c_c$, where a and b are the inner and outer radii of the collar, respectively. The specimen is assumed to be "soft" if, after contact ($t = t_1^+$), $\bar{\sigma}_r$ remains zero and the radial strain rate at the specimen-collar interface ($\dot{\bar{\epsilon}}_r$) changes discontinuously to zero. The specimen is assumed to be "rigid" if, after contact ($t = t_1^+$), $\bar{\epsilon}$ retains its precontact value and $\bar{\sigma}_r$ changes discontinuously to a finite value (for details see the Appendix). J_2 is the second invariant of the stress deviator tensor. W^p is the plastic work. E_s and ν_s are Young's modulus of elasticity and Poisson's ratio of the specimen.

3. SPECIMEN MATERIAL SELECTION AND PREPARATION

A sample of both metallics and non-metallics were selected for tests. A variety of aluminum alloys (3003, 2024-T351 and 6061-T651) and oxygen-free copper constituted the metallic category; and Scotchply (a glass-filament reinforced resin), syntactic foam (hollow glass microspheres embedded in epoxy resin), and polypropylene panels made up the non-metallic category. All samples from metallic materials were cut perpendicular to the rolling direction of the rod. Metallographic studies[9] showed significant elongation of the grains in the rolling direction, and a more complete test should include transverse specimens as well.

The Scotchply consisted of layers of unidirectionally oriented filaments, each layer rotated 120° with respect to its predecessor, to achieve a transversely isotropic material after curing. For this material specimens were cut so that the loading axis was either parallel or perpendicular to the planes making up the filament layers. Polypropylene panel consisted of reinforced layers normal to axial loading. Syntactic foam specimens were cut parallel to the edges of the block. Although the disk-shaped specimens were machined to a nominal thickness of 13 mm (final dimension was recorded to four significant figures), much greater care was devoted to the radial dimension. To assure minimum clearance between specimen and collar, the specimen diameter was machined to 38.295 mm. Since the minimum diameter in the collar is 38.299 mm, the total clearance was limited to 4.0 μm. To simplify insertion of the specimen into the collar, metallic specimens were usually kept in a freezer prior to use. Testing was then carried out after the specimen has been allowed to reach room temperature.

Care was taken to assure flatness and parallelism of the specimen. In the metallic specimens, a surface flatness was such that less than 400 nm variation was present over the ~38 mm diameter (identical to the finish on the ends of the input and output bars), and specimen faces were parallel to within 40 sec of arc. Pre-test misalignment between specimen and bars was less than 25 sec of arc.

4. EXPERIMENTAL RESULTS

Axial stress–strain curves were obtained for all materials using the Kolsky formulas (eqns 1 and 2). Data reduction consisted of visually digitizing the oscilloscope traces at 2 μs intervals. After synchronization of the reflected and output signals relative to the input signal by means of a 41.5 μs delay time t_d, the digitized data were read into a computer program[9]. The program averaged and integrated the data in accordance with eqns (1) and (2). The results are shown in Figs. 4–12. Two sets of curves are presented in each graph: constrained (specimen restrained by the collar, labelled CD); and unconstrained (collar absent, labelled UD). The stiffening effect of the collar is apparent except at low stress levels before the specimen makes contact with the collar. Axial strains at contact vary from 0.1% for 2024–T351 Al to 2% for polypropylene. The contact point was established by the intersection of the tangent moduli at low and intermediate stress levels.

The radial clearance strain ϵ_1 associated with the axial contact strain may be estimated using the definition of Poisson's ratio, $\nu = -\epsilon_1/\epsilon_z$. Here it is assumed that the specimen is in a state of uniaxial stress prior to contact (ideal lubrication between the faces of the specimen and the bars). Taking 0.3 as a reasonable value for ν, we conclude that the radial clearance strain ranges from 0.03% for 2024-T351 Al to 0.6% for polypropylene. Since the specimen diameter is $a = 38$ mm, the estimated diametral expansion is 11 μm for the aluminum and 228 μm for the polypropylene. The smaller figure shows fair agreement with the tolerance of 4.0 μm specified in Section 3. The larger figure for the polypropylene is due to the fact that these specimens were prepared early in the test program, well before the need for such close tolerances was recognized.

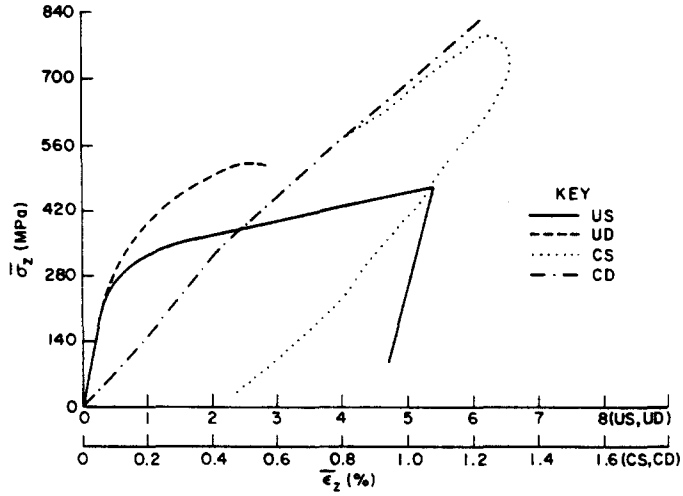

Fig. 4. Axial stress–strain curves for 2024-T351 Al.

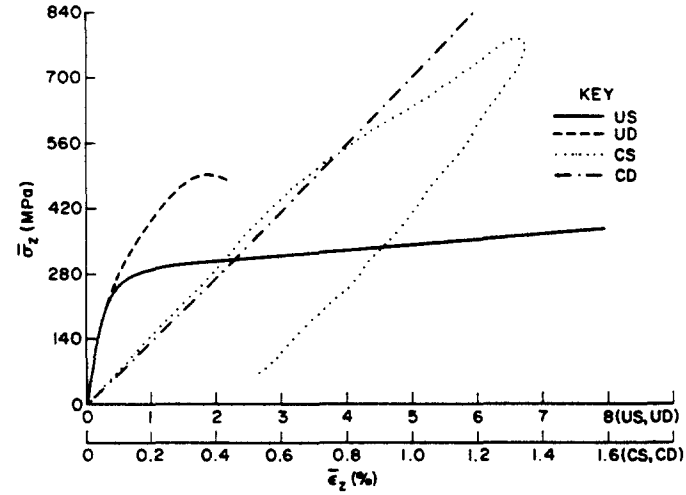

Fig. 5. Axial stress–strain curves for 6061-T651 Al.

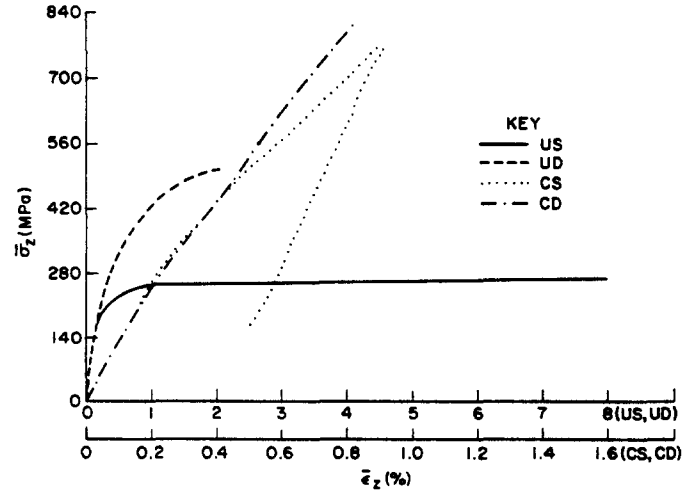

Fig. 6. Axial stress–strain curves for oxygen-free copper.

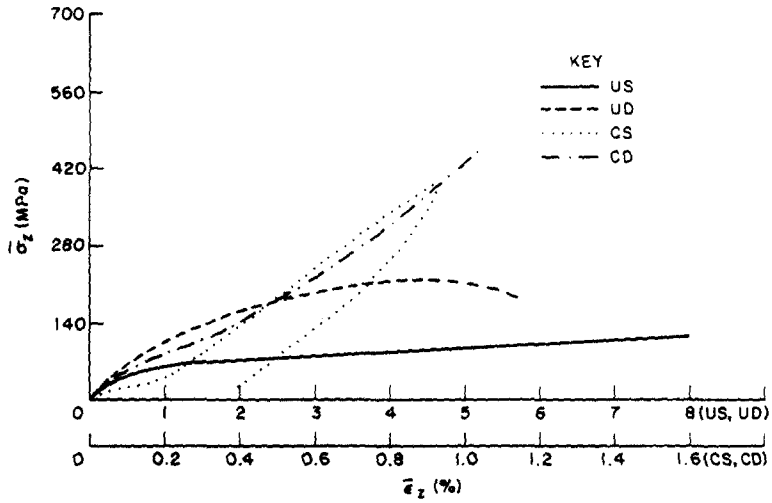

Fig. 7. Axial stress–strain curves for 3003 Al (as received).

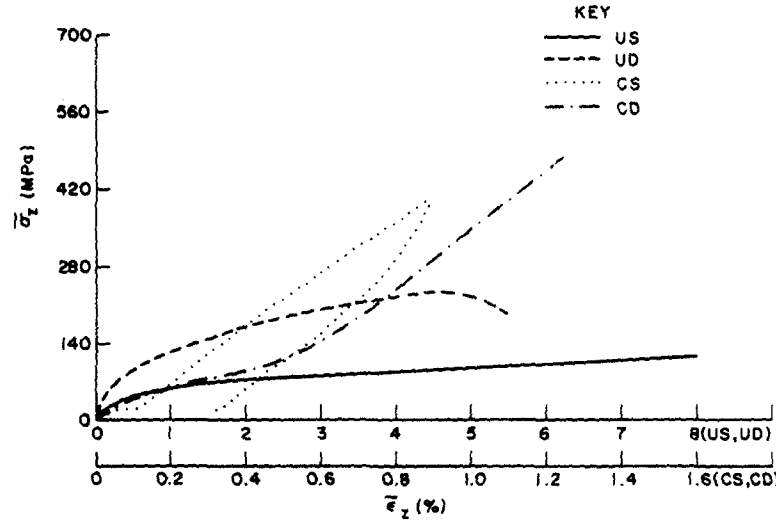

Fig. 8. Axial stress–strain curves for 3003 Al (annealed).

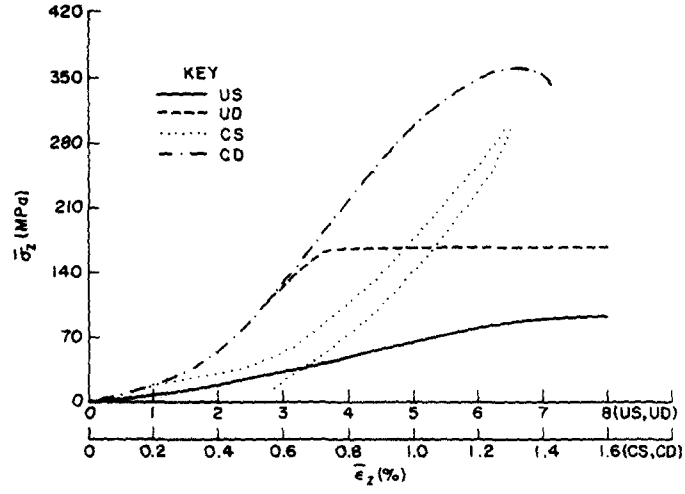

Fig. 9. Axial stress–strain curves for polypropylene.

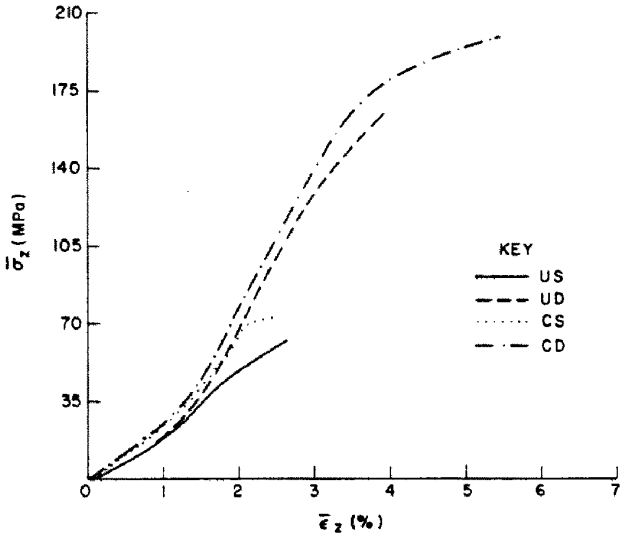

Fig. 10. Axial stress–strain curves for syntactic foam.

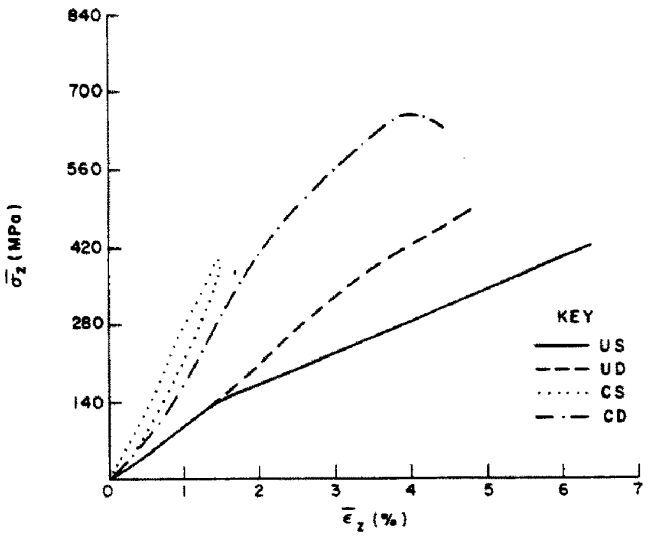

Fig. 11. Axial stress–strain curves for Scotchply (load normal to plies).

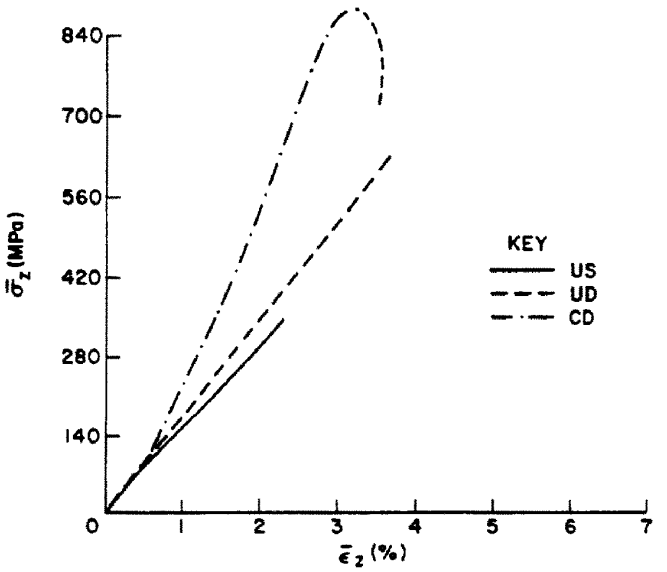

Fig. 12. Axial stress–strain curves for Scotchply (load parallel to plies).

To facilitate comparison, curves obtained from the static tests described in Ref. [9] are also presented in Figs. 4–12. Constrained specimen curves are labelled CS, and unconstrained specimen curves are labelled US. The rate effect is observable in the unconstrained specimens, while the restraint offered by the collar appears to suppress, if not reverse, the effect. In the static tests, strain rates are on the order of $10^0\,s^{-1}$ or less, while in the dynamic tests, strain rates generally exceed $10^3\,s^{-1}$. Lack of consistent results between unconstrained and constrained specimen behavior will be discussed in the next section.

By means of eqn (3), the radial stress history can be calculated for the metallic specimens. Cross-plotting these data with the axial stress history provides a stress trajectory in principal stress space. Trajectories are shown in Fig. 13 for oxygen-free copper. It is seen that the trajectory consists first of a uniaxial stress path ($\sigma_r = 0$) before the specimen makes contact with the collar. After contact, the trajectory turns abruptly toward the space diagonal ($\sigma_r = \sigma_z$), with the degree of abruptness determined by the rigidity of the specimen relative to the collar. It is seen that the rigidity effect (see the Appendix for more details) is only temporary; at later times (larger stress levels), the influence of the initial clearance becomes negligible on the stress trajectory.

However, at the lower stress levels, the desirability of vanishing radial clearance becomes apparent. With zero clearance, a truly biaxial trajectory will begin at the origin, and ambiguity regarding "rigid" or "soft" specimen behavior is avoided completely. Calculated static stress trajectories are also shown in Fig. 13. Values of radial stress are found using eqn (14) in the Appendix and a value of 280 GPa for the collar modulus E_c. The value was obtained by a finite element analysis of the collar in conjunction with curve fitting of the static uniaxial stress and uniaxial strain data, (see Ref. [9]). Although the static and dynamic trajectories are similar at larger stress levels, substantial differences occur at lower stresses because of radial clearance (static contact vs dynamic impact). The need for vanishing radial clearance is again apparent.

Knowledge of the biaxial stress and strain histories enables the determination of the hardening curves for the metallic specimens by means of eqns (1)–(5). Results of these calculations are shown in Figs. 13–18. Both static and dynamic curves are presented for both constrained and unconstrained specimens. It is seen that the hardening curves for the specimens tested statically (constrained and unconstrained) show reasonable agreement. (Calculations of effective plastic strain and effective stress follow the steps outlined in the Appendix.) Significant differences are found in the dynamic curves, where the rate effect is pronounced. In all cases the unconstrained dynamic data show the greatest departure from the static data. This

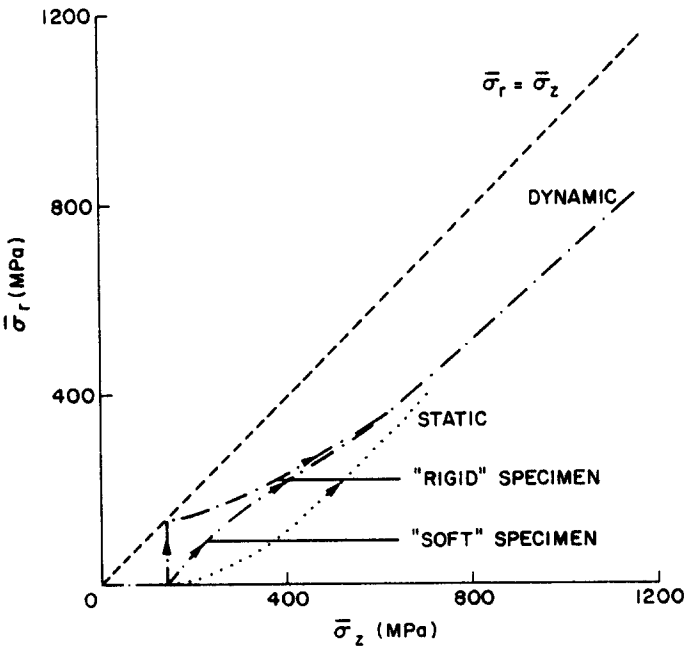

Fig. 13. Stress trajectories for oxygen-free copper.

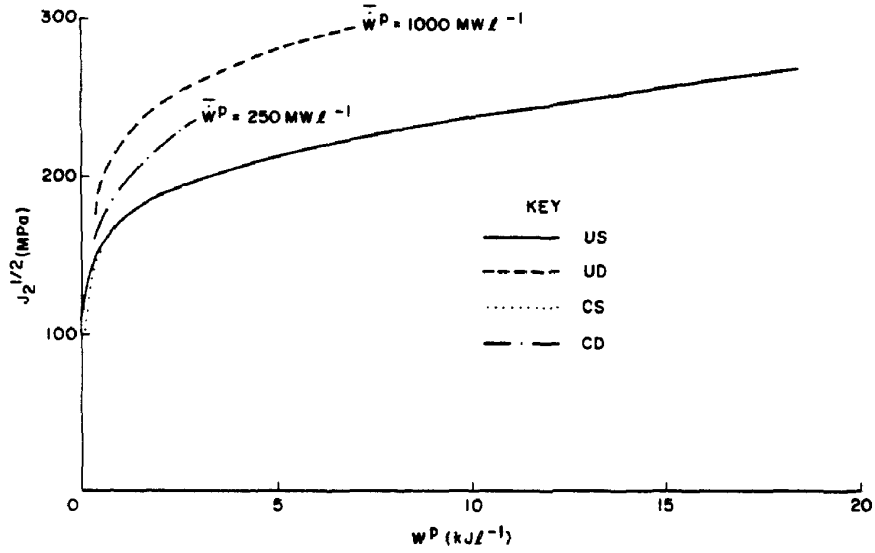

Fig. 14. Hardening curves for 2024-T351 Al.

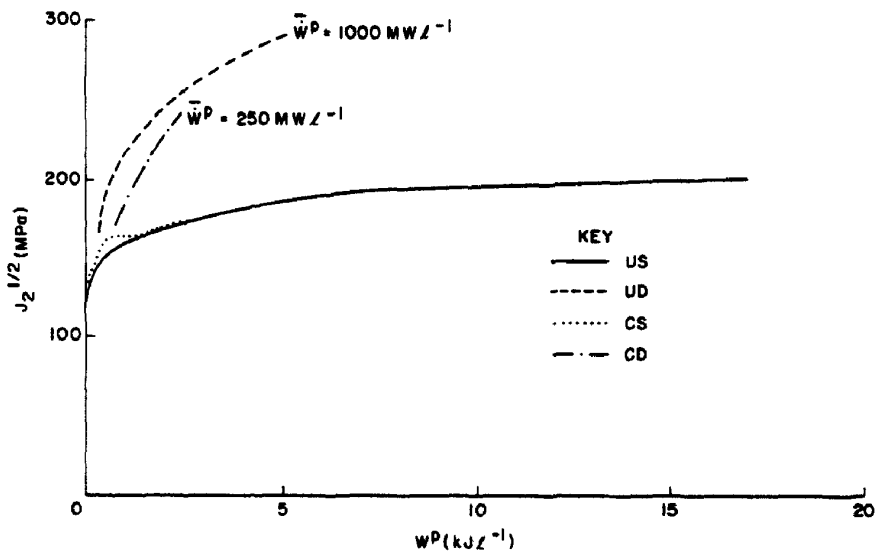

Fig. 15. Hardening curves for 6061-T651 Al.

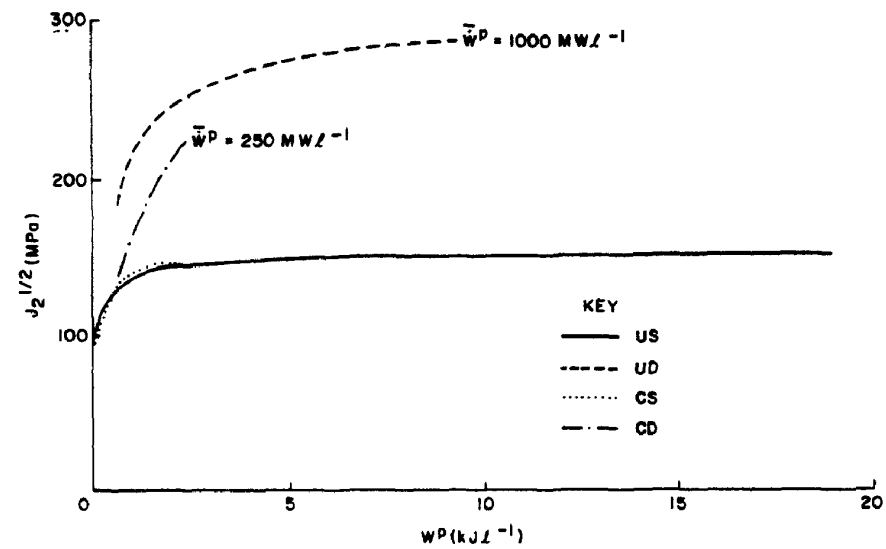

Fig. 16. Hardening curves for oxygen free copper.

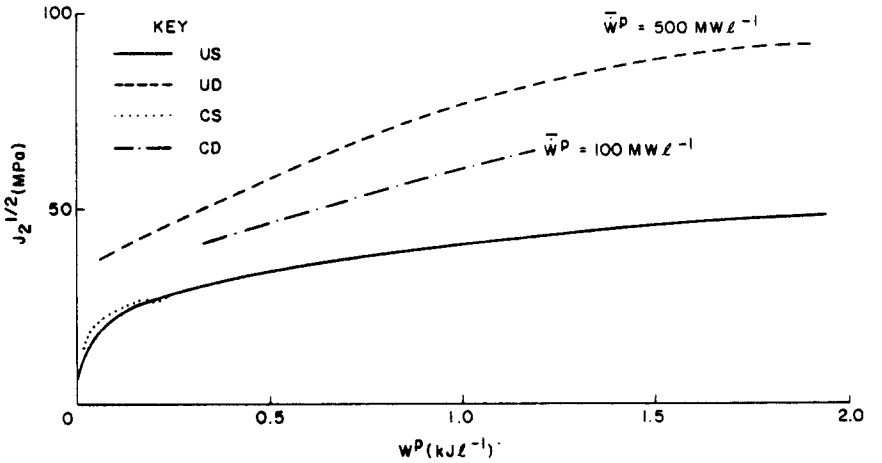

Fig. 17. Hardening curves for 3003 Al (annealed).

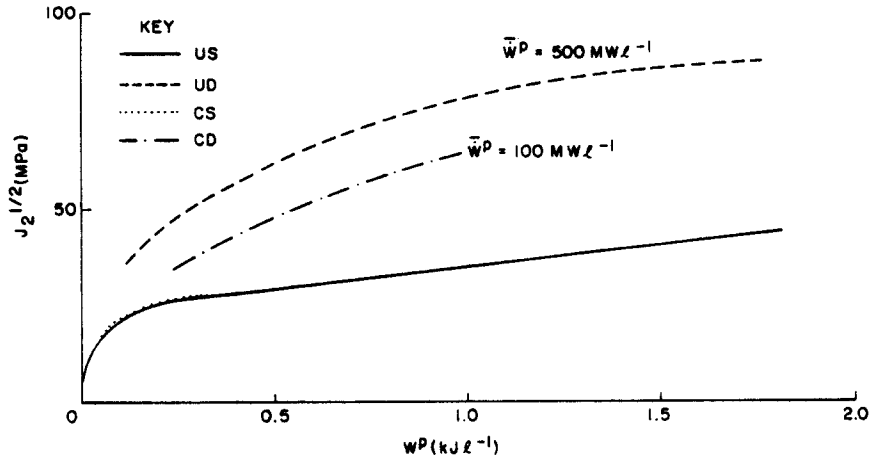

Fig. 18. Hardening curves for 3003 Al (as received).

behavior is to be expected since the strain rates are the highest in the unconstrained specimens, usually on the order of 3000 s^{-1}. The constrained dynamic data form an intermediate curve; in this case the strain rate is approximately 1000 s^{-1}.

Metallographic studies were carried out to compare the grain deformation behavior of metals tested under static uniaxial stress and strain with that of specimens tested dynamically. A specimen was cut from the stock of the metal to be studied, then mechanically polished, etched and examined under the microscope. The appearance of a virgin specimen was compared with the published data for consistency. Comparison of the photographs before and after testing shows little difference in the appearance. This result is to be expected since the plastic deformation is limited usually to less than 10% (for photographs see Ref. [9]).

5. DISCUSSION AND CONCLUSIONS

It appears that the collar-modified Kolsky apparatus can be used with some confidence to determine the dynamic compressive behavior of materials under conditions approaching uniaxial strain. When the materials are ductile metals undergoing no plastic volume change, the information provided by the strain gage records on the input and output bars enables the calculation of radial as well as axial stress and strain histories. With other materials, a suitably sensitive collar gage is needed to supplement the bar gage data. At the present time, background noise almost obliterates the collar gage signal, and further improvement in gage factor and in noise filtering is needed before an accurate record of radial stress and/or strain history of the specimen can be deduced. Completion of this development phase is required before the collar-modified apparatus can provide quantitative radial data for non-metallics such as concre, rocks and other earth materials.

Attention must be drawn to the fact that the experimental data reported here consistently show a rate effect, not only for the annealed alloy metals but for the tempered alloys of aluminum as well. Thus, while qualitative agreement is found with the results of Refs. [2, 3, 5, 6 and 10–16] for 3003 Al, 2024-T351 Al and oxygen-free copper, the rate dependence for 6061-T651 Al reported here is not confirmed by the data published in Refs. [3 and 10]. On the other hand, the tensile data reported in Refs. [17 and 18] supports the existence of a rate dependent material behavior for 6061-T6 Al, although a very different test technique (expanding ring) was used to obtain these results. Another explanation may lie in the Kolsky formulas (eqns 1 and 2) used to reduce the data. These formulas are based on the assumption of stress uniformity along the specimen, an assumption which may be violated at the higher rates of strain. However, an analysis based on Ref.[19] and the results of Ref.[20] indicate that eqns (1) and (2) give suitable *average* stress–strain relationships for rate-independent metals until the maximum stress is reached. Beyond this point, wave effects dominate and a more exact analysis is required. For this reason, the dynamic data are not continued beyond the point of maximum stress. Departures from the static hardening curves are obvious for both the constrained and the unconstrained specimens. Hence, it is concluded that the rate dependence is real for all metals tested.

Acknowledgement—The research reported here is based on a portion of a doctoral thesis of Dr. Bhushan. Financial support was provided in part by a grant from the National Science Foundation and University Graduate Fellowship.

REFERENCES

1. H. Kolsky, An investigation of the mechanical properties of materials at very high rates of loading. *Proc. Phys. Soc.* **B62**, 676–700 (1949).
2. U. S. Lindholm, Some experiments with the split Hopkinson pressure bar. *J. Mech. Phys. Solids* **12**, 317–335 (1964).
3. U. S. Lindholm and L. M. Yeakley, High strain-rate testing: tension and compression. *Exp. Mech.* **8**, 1–9 (1968).
4. E. D. H. Davies and S. C. Hunter, The dynamic compression testing of solids by the method of the split Hopkinson pressure bar. *J. Mech. Phys. Solids* **11**, 155–179 (1963).
5. W. E. Baker and C. H. Yew, Strain-rate effects in the propagation of torsional plastic waves. *J. Appl. Mech.* **33E**, 917–923 (1966).
6. J. Duffy, J. D. Campbell and R. H. Hawley, On the use of a torsional split Hopkinson bar to study rate effects in 1100-0 aluminum. *J. Appl. Mech.* **38E**, 83–91 (1971).
7. J. M. Walsh, M. H. Rice, R. G. McQueen and F. L. Yarger, Shock-wave compression of twenty-seven metals. Equation of state of metals. *Phys. Rev.* **108**, 196–216 (1957).
8. W. E. Jahsman, The Kolsky apparatus for the measurement of dynamic material properties *CUMER*-68-3, (July 1968).
9. B. Bhushan, Experimental and numerical studies of rate-dependent materials, Ph.D. Thesis, University of Colorado, Boulder (April 1976).
10. D. L. Holt, S. G. Babcock, S. J. Green and C. J. Maiden, The strain-rate dependence of flow stress in some aluminum alloys. *Trans. ASME* **60**, 152–159 (1967).
11. T. Nicholas, Strain-rate and strain-rate-history effects in several metals in torsion. *Exp. Mech.* **11**, 370–374 (1971).
12. C. H. Karnes and E. A. Ripperger, Strain rate effects in cold worked high-purity aluminum. *J. Mech. Phys. Solids* **14**, 75–88 (1966).
13. S. K. Samanta, Dynamic deformation of aluminium and copper at elevated temperatures. *J. Mech. Phys. Solids* **19**, 117–135 (1971).
14. K. Kishida and K. Senda, New experimental method for determining dynamic stress–strain relation of metals. *Exp. Mech.* **8**, 567–571 (1968).
15. T. Nicholas and J. E. Lawson, On the determination of the mechanical properties of materials of high strain rates. *J. Mech. Phys. Solids* **20**, 57–64 (1972).
16. C. K. H. Dharan and F. E. Hauser, Determination of stress–strain characteristics at very high strain rates. *Exp. Mech.* **10**, 370–376 (1970).
17. C. R. Hoggatt and R. F. Recht, Stress–strain data obtained at high rates using an expanding ring. *Exp. Mech.* **9**, 441–448 (1969).
18. K. G. Hoge, Influence of strain rate on mechanical properties of 6061-T6 aluminum under uniaxial and biaxial states of stress. *Exp. Mech.* **6**, 204–211 (1966).
19. W. E. Jahsman, Reexamination of the Kolsky technique for measuring dynamic material behavior. *J. Appl. Mech.* **38E**, 75–82 (1971).
20. L. D. Bertholf and C. H. Karnes, Two-dimensional analysis of the split Hopkinson pressure bar system. *J. Mech. Phys. Solids* **23**, 1–19 (1975).

APPENDIX: AXISYMMETRIC STRESS–STRAIN BEHAVIOR

Static collar response

Let z and r denote axial and radial coordinates (Fig. 19). For small deformations the elastic and plastic strains are additive,

$$\epsilon_z = \epsilon_z^e + \epsilon_z^p \tag{6}$$

$$\epsilon_\theta = \epsilon_r = \epsilon_r^e + \epsilon_r^p. \tag{7}$$

Due to axisymmetric loading, σ_r is equal to σ_θ.

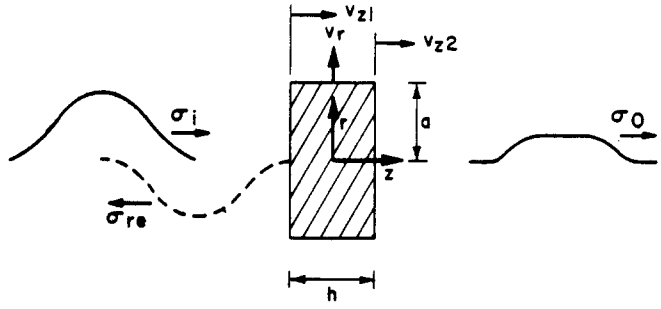

Fig. 19. Specimen coordinates.

Therefore elastic strains are related to stresses as

$$\epsilon_z^e = \frac{1}{E_s}[\sigma_z - 2\nu_s\sigma_r] \tag{8}$$

$$\epsilon_r^e = \frac{1}{E_s}[(1-\nu_s)\sigma_r - \nu_s\sigma_z] \tag{9}$$

where E_s is Young's modulus and ν_s is the Poisson's ratio of the specimen.

For a ductile material obeying the von Mises yield condition and Prandtl–Reuss flow rule, we have the expressions for the second invariant of the stress deviator, J_2, and plastic work, W^p:

$$\sqrt{J_2} = \frac{1}{\sqrt{3}}[\sigma_z - \sigma_r] \tag{10}$$

$$\epsilon_z^p = -2\epsilon_r^p \tag{11}$$

$$W^p = \int_0^{\epsilon_z^p} \sqrt{(3J_2)}\, d\epsilon_z^p. \tag{12}$$

We define the collar constraint parameter E_c as

$$-\sigma_r/E_c = \epsilon_r - \epsilon_1 \tag{13}$$

where ϵ_1 is the clearance strain and is given by the radial clearance between the specimen and the collar divided by the specimen radius. From eqns (6)–(13) we obtain

$$\frac{1}{E_s}\sigma_r = \frac{1}{1-2\nu_s+(E_s/E_c)}\left\{\epsilon_1 + \frac{1}{2}\epsilon_z - \frac{(1-2\nu_s)}{2E_s}\sigma_z\right\} \tag{14}$$

$$\epsilon_z^p = \frac{1}{1-2\nu_s+(E_s/E_c)}\left\{2\nu_s\epsilon_1 + (1-\nu_s+E_s/E_c)\,\epsilon_z - \frac{(1-\nu_s-2\nu_s^2+E_s/E_c)}{E_s}\sigma_z\right\}. \tag{15}$$

Measured values are σ_z, ϵ_z and ϵ_1. With that set of data and the help of eqns (14) and (15) we calculate σ_r and ϵ_z^p. We can then determine $\sqrt{(J_2)} - W^p$ curves with the help of eqns (10) and (12).

Dynamic collar response

Figure 19 represents a free body diagram of the specimen of thickness h and radius a which is surrounded by a collar during testing. Polar coordinates (r, z) are used here. σ_i, σ_{re} and σ_0 are the time-dependent incident, reflected, and transmitted stress pulses, respectively. v_{z1} and v_{z2} are the axial particle velocities of front and rear surfaces of the specimen. v_r is the radial particle velocity of the specimen surface making contact with the collar.

The conventional Kolsky formulas (eqns 1 and 2) for such a problem are given by

$$\bar{\dot{\epsilon}} = \frac{v_{z2} - v_{z1}}{h} \tag{16}$$

$$= \frac{1}{(\rho c)_b h}[-\sigma_0 + (\sigma_i - \sigma_{re})] \tag{17}$$

$$= \frac{2}{(\rho c)_b h}(\sigma_i - \bar{\sigma}_z) \tag{18}$$

where $(\rho c)_b$ is the acoustic impedance of the bar.

Similar equations are developed for the radial motion,

$$\bar{\dot{\epsilon}}_r = \frac{v_r}{a} \tag{19}$$

$$\bar{\sigma}_r = \begin{cases} -(\rho c)_c v_r - E_c(\bar{\epsilon}_r - \epsilon_1), & \bar{\epsilon}_r > \epsilon_1 \\ 0, & \bar{\epsilon}_r < \epsilon_1 \end{cases} \tag{20}$$

where $(\rho c)_c$ is the acoustic impedance of the collar and c_c^2 is defined by E_c/ρ_c. The second term in eqn (20) represents the effective collar restraint and is consistent with eqn (13).

Equations (19) and (20) are combined to

$$\bar{\sigma}_r = -D\bar{\epsilon}_r + E_c\epsilon_1 \tag{21}$$

where D is the linear operator $(\rho c)_c\, a\,(\mathrm{d}/\mathrm{d}t) + E_c$. The operator D is applied to the dilation $\bar{\epsilon}_z + 2\bar{\epsilon}_r$ (axisymmetric deformation) and eqns (6) and (7) are used to obtain

$$D(\bar{\epsilon}_z + 2\bar{\epsilon}_r) = D(\bar{\epsilon}_z^{\,e} + 2\bar{\epsilon}_r^{\,e}) + D(\bar{\epsilon}_z^{\,p} + 2\bar{\epsilon}_r^{\,p}). \tag{22}$$

For ductile metals there is no plastic volume change ($\bar{\epsilon}_z^{\,p} + 2\bar{\epsilon}_r^{\,p} = 0$). Using eqns (8) and (9) for ductile metals with eqn (22) we get

$$D(\bar{\epsilon}_z + 2\bar{\epsilon}_r) = D(\epsilon_z^{\,e} + 2\epsilon_r^{\,e}) = D\left\{\frac{1-2\nu_s}{E_s}(\bar{\sigma}_z + 2\bar{\sigma}_r)\right\}. \tag{23}$$

Using eqns (18), (21) and (23) we solve for $\bar{\sigma}_r$ in terms of known variables,

$$\left[D\frac{1-2\nu_s}{E_s} + 1\right]\bar{\sigma}_r = \frac{(\rho c)_c a}{(\rho c)_b h}(\sigma_i - \bar{\sigma}_z) - \left[D\frac{1-2\nu_s}{2E_s}\right]\bar{\sigma}_z + E_c\left(\frac{1}{2}\bar{\epsilon}_z + \epsilon_1\right). \tag{24}$$

Introducing the new parameter, $\alpha = E_c(1-2\nu_s)/E_s$, $\tau_1 = (a/c_c)\,\alpha/(1+\alpha)$, and $\chi = (\rho c)_c\, a/(\rho c)_b h$, we can write (24) as

$$\frac{\mathrm{d}\bar{\sigma}_r}{\mathrm{d}t} + \frac{1}{\tau_1}\bar{\sigma}_r = -\frac{1}{2}\left(\frac{\mathrm{d}\bar{\sigma}_z}{\mathrm{d}t} + \frac{1}{\tau_1}\bar{\sigma}_z\right) + \frac{1}{\tau_1(1+\alpha)}\left[\chi(\sigma_i - \bar{\sigma}_z) + \frac{1}{2}(E_c\bar{\epsilon}_z + \bar{\sigma}_z) + E_c\epsilon_1\right]. \tag{25}$$

Let the time at which contact takes place (i.e. $\epsilon_r = \epsilon_1$) be t_1. Integrating eqn (25) we get

$$\bar{\sigma}_r = \left[\bar{\sigma}_r(t_1) + \frac{1}{2}\bar{\sigma}_z(t_1)\right]\bar{e}^{(t-t_1)/\tau_1} - \frac{1}{2}\bar{\sigma}_z(t) + \frac{1}{\tau_1(1+\alpha)}\int_{t_1}^{t}\chi(\sigma_i - \bar{\sigma}_z) + \frac{1}{2}(E_c\bar{\epsilon}_z + \bar{\sigma}_z + 2E_c\,\epsilon_1)\,\bar{e}^{(t-t')/\tau_1}\,\mathrm{d}t'. \tag{26}$$

The only unknown in eqn (26) is $\bar{\sigma}_r(t_1)$ which is obtained from eqns (19) and (20),

$$\bar{\sigma}_r(t_1) = -(\rho c)_c\, a\bar{\epsilon}_r(t_1). \tag{27}$$

Before the contact ($t \le t^-$), $\bar{\sigma}_r = 0$ and from eqns (6)–(9),

$$\bar{\epsilon}_r(t_1) = \frac{1}{2}\left[-\bar{\epsilon}_z(t_1) + \frac{(1-2\nu_s)}{E_s}\bar{\sigma}_z(t_1)\right]. \tag{28}$$

After contact ($t = t_1^+$) there are two limiting cases: $\bar{\sigma}_r$ remains zero and $\bar{\epsilon}_r$ changes discontinuously to zero to satisfy eqn (27); $\bar{\epsilon}_r$ retains its pre-contact value and $\bar{\sigma}_r$ jumps instantly to a finite value from its previous zero value following the eqn (27).

For the latter case from eqns (27), (28) and (18) we get,

$$\bar{\sigma}_r(t_1^+) = -(\rho c)_c\frac{a}{2}[-\bar{\epsilon}_z(t_1) + (1-2\nu s)\,\bar{\sigma}_z(t_1)/E_s] = \chi(\sigma_i(t_1) - \bar{\sigma}_z(t_1)) - \tau_1(1+\alpha)\bar{\sigma}_z(t_1)/2. \tag{29}$$

If the specimen is elastic at $t = t_1$, eqn (29) reduces to

$$\bar{\sigma}_r(t_1^+) = 2\nu_s\chi(\sigma_i(t_1) - \bar{\sigma}_z(t_1)). \tag{30}$$

Equations (17), (18), (28)–(30), (10) and (12) are used to reduce the axial stress–strain curves to $\sqrt{(J_2)} - W^p$ curves.